nature communications

Article

https://doi.org/10.1038/s41467-025-61512-8

Attosecond X-ray spectroscopy reveals the competing stochastic and ballistic dynamics of a bifurcating Jahn–Teller dissociation

Received: 29 November 2024

Accepted: 23 June 2025

Published online: 16 July 2025

Check for updates

Danylo Matselyukh [1], Vít Svoboda [1,2] & Hans Jakob Wörner [1]

A fundamental approach to understanding chemical processes involves two key concepts: reaction paths and vibrational wavepackets. Collecting sufficient observables to experimentally determine these paths still challenges the latest advances in ultrafast science. Simultaneously observing the coherent nature of the wavepacket following them is even more challenging. Here, exploiting the sub-femtosecond time resolution ($\sigma = 1$ fs) of attosecond soft-X-ray-absorption spectroscopy, we overcome both of these challenges and observe a Jahn-Teller-mediated chemical reaction in its entirety—from initial symmetry breaking to beyond dissociation. We find that the Jahn-Teller effect in SiH_4^+ immediately bifurcates the reaction into two channels: ballistic dissociation into SiH_3^+ and H in 22.9 ± 0.5 fs in which the vibrational wavepacket is preserved, and—after an induction time of 11 ± 3.4 fs—a stochastic dissociation into SiH_2^+ and H_2 with a timescale of 140 ± 19 fs in which the wavepacket dephases. We find that adiabatic ab-initio molecular dynamics simulations correctly reproduce the ballistic channel, but fail with the stochastic channel. These unprecedented insights into an ultrafast Jahn-Teller-mediated chemical reaction establish the unique potential of our experimental scheme for investigating chemical processes, particularly ones containing non-adiabatic dynamics or involving hydrogen atoms, which are notoriously difficult to detect with other methods, such as electron or X-ray diffraction.

The Jahn–Teller (JT) distortion may be one of the most interesting physical processes in chemical physics due to its ubiquity in nature and implications. As a result, it has been studied in detail for more than 80 years (see refs. 1,2 and references therein), mainly with time-independent methods. According to the JT theorem, any non-linear molecule in an electronically degenerate state will undergo a structural distortion that removes this degeneracy[3]—as the only precondition is electronic degeneracy, JT distortions appear everywhere: in material science, molecular spectroscopy, the properties of transition-metal complexes, and even in the superconductivity of unconventional superconductors[4].

The predictions of the JT theorem are, however, limited to the geometric vicinity of the degeneracy. Dynamics and observables further away from this high-symmetry point can be very diverse and complex. The methane cation is an excellent example hereof: correctly understanding the cation's vibrational spectrum requires careful consideration of tunnelling[5] and geometric phase effects[6]. Moreover, the reaction path describing the JT distortion upon ionisation of neutral methane is debated: similar experimental studies coming to different conclusions when supported with different ab-initio quantum chemistry simulations[7–9].

Resolving such disputes is critical to our understanding of ultrafast non-adiabatic processes and requires an ultrafast methodology with less reliance on advanced (and somewhat black-box) ab-initio simulations. We propose our novel attosecond soft-X-ray (SXR) transient-absorption spectroscopy (TAS) coupled with in-situ mass

[1]Laboratorium für Physikalische Chemie, ETH Zürich, Zürich, Switzerland. [2]Department of Physical Chemistry, University of Chemistry and Technology, Prague, Prague, Czech Republic. e-mail: hwoerner@ethz.ch

spectrometry (MS) as a solution. While femtosecond SXR TAS, which has been used in studies of the JT effect in tetrahedral and octahedral systems[10,11], is able to capture the population dynamics and end-products of chemical processes, the increased time resolution of attosecond TAS (ATAS) allows individual vibrational quantum beats to be resolved, providing unique insights on the reaction path. This has been seen in the studies on the methane cation[7,8], however, the rapid dephasing of the single experimental observables (or the drop of its amplitude below the noise floor of the measurement) have prevented the reaction path from being conclusively determined.

In this work, we improve the energy resolution and signal-to-noise ratio (SNR) by studying the silicon L-edge (particularly core-Rydberg transitions) instead of core-valence transitions at the carbon K-edge. Additionally, coupling ATAS with MS provides a robust secondary observable to which the ATAS measurements can be referenced, reducing the reliance on ab-initio simulations.

With this novel approach we successfully resolve and assign the complete vibrational dynamics (including their coherent or statistical nature) of one of the fastest possible chemical processes—the JT distortion of silane cation—all the way from initiation to equilibration. By observing the dynamics of the silane cation with sub-femtosecond resolution, we identify and follow the quantum beats of the dissociating vibrational wavepackets in two separate channels, and isolate the spectra of transient species that are only present for a few femtoseconds. Furthermore, we provide the first experimental evidence for the JT-induced bifurcation of a chemical reaction. To date, such vibrational bifurcations have only been predicted and observed in adiabatic dynamics at valley ridge inflection points[12,13]; bifurcations between the spin-orbit states of iodine- and bromine-containing molecules have also been resolved[14,15] but share common reaction paths and do not lead to chemically distinct products.

Results and discussion

The SXR-ATAS experimental methodology employed in this work builds on ref. 16, with the addition of an in-situ time-of-flight mass spectrometer (TOF-MS) which allows for the identification of the charged fragments generated through strong-field ionisation (SFI) independently from the SXR absorption spectra (see Supplementary Section S1 for experimental details). In short, starting from the tetrahedral silane molecule (SiH_4) in its electronic ground state, we suddenly activate the JT effect by strong-field-ionising the triply-degenerate highest-occupied molecular orbital (HOMO) with an optical (500–1000 nm) laser pulse. The ultrafast vibrational dynamics that this launches in SiH_4^+ are probed with SXR absorption using an isolated sub-200-as pulse covering the silicon-$L_{2,3}$ edge. This experimental scheme yields a cross-correlation with a standard deviation of just $\sigma = 1.00 \pm 0.05$ fs (or 2.37 ± 0.13 fs in full width at half maximum measured in xenon, see Supplementary Fig. S1). The experimental XAS are processed using a singular-value based filtering (Supplementary Section S1.3) and interpreted with the help of previous synchrotron studies[17] and our MS results.

The experimental data are presented in Figs. 1b and 2a. The first shows a picosecond-spanning measurement that captures the entire dissociation of SiH_4^+, whereas the second shows a finer delay-step measurement in which the initial vibrational dynamics are more clearly visible. A lower energy range of the latter dataset was also the subject of ref. 16.

Before unravelling the JT dynamics of SiH_4^+, we first examine the 15-fs-period signals that dominate the 102.5–107.5 eV region of the transient spectrum. These are the result of Si–H stretching vibrations in the electronic ground state of SiH_4, illustrated on the left-hand side of Fig. 1b. As the measured vibrational wavepacket is not found to be displaced immediately after $\Delta t = 0$, and based on comparisons with the literature[14,18,19], we determine that these dynamics are initiated through bond softening. These coherent observables also serve as a proverbial canary: their constant amplitude across all delays assures us that

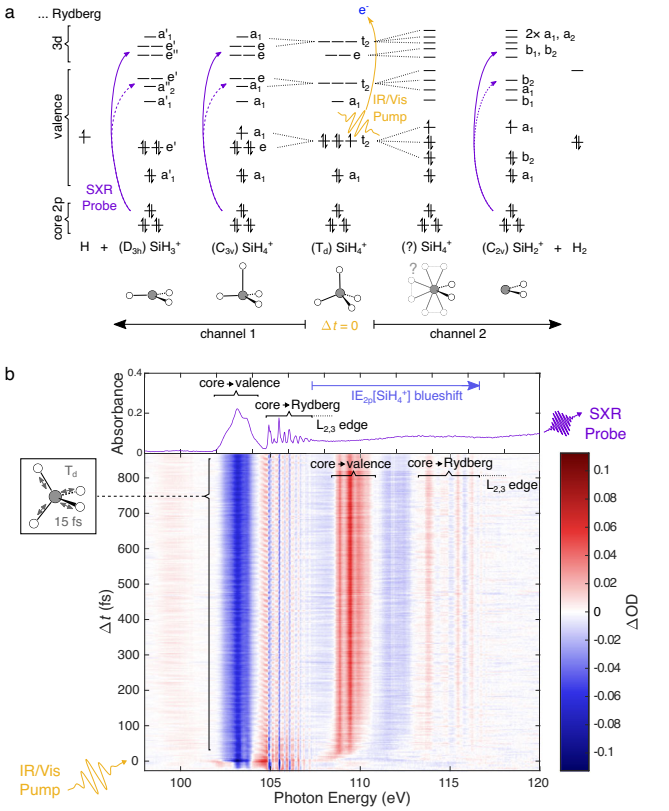

Fig. 1 | Overview of the chemical system and the ATAS results. a Schematic of the orbital structure of SiH_4^+ and its fragments. The energetic ordering, occupation and symmetry of the orbitals of SiH_4^+ and its fragments in various relevant geometries is shown. The SFI pump process is represented with a yellow arrow while the XAS (probe) transitions are represented by purple lines. Solid lines indicate the dominant observed transitions. **b** The results of an ATAS measurement on silane, whose measured static absorption is plotted in the top panel. The core-valence (102–104.5 eV) and core-Rydberg (104.5–107.5 eV) transitions of SiH_4 are clearly separated, with the latter showing far narrower features. The blueshift of the $L_{2,3}$-absorption edge of the cationic species (shown as a blue arrow) is discussed in Supplementary Section S2.2.

modulations in other vibrational quantum beats are not coherent artefacts induced by the pump-pulse pedestal.

We now turn to SiH_4^+. Upon ionisation of the HOMO of silane, the JT effect lowers the energy of the system by breaking its T_d symmetry, raising the energy of the SOMO and lowering that of the doubly-occupied orbitals (Fig. 1a). In contrast to the methane cation, which is readily observed in its unfragmented form[20], the JT-relaxation in SiH_4^+ leads to dissociation into SiH_3^+ or SiH_2^+ ions[21]. Measurements from our in-situ TOF-MS at various pump intensities (Supplementary Fig. S2) reveal the products of SFI to be always dominated by approximately equal amounts of SiH_3^+ and SiH_2^+. This agrees with non-time-resolved ionisation studies[21,22] and demonstrates that the use of few-cycle SFI does not significantly modify the fragmentation ratio of SiH_4^+ compared to above-threshold single-photon ionisation. This is particularly important for the analysis of the SiH_2^+ channel as it ensures that the energetically-forbidden sequential fragmentation channel $SiH_4^+ \rightarrow SiH_2^+ + H + H$ remains closed for our experimental conditions.

The XAS of these fragments can be observed in our ATAS results, showing excellent agreement with previous synchrotron studies[17,23]. Ionisation leads to a large change in the overall structure of the SiH_n^+ $L_{2,3}$-edge XAS. While the absorption spectrum of silane exhibits only two distinct regions (2p → anti-bonding below 104.5 eV and 2p → Rydberg above[23]), the ionic species exhibit three[17] (a 2p → anti-bonding

https://doi.org/10.1038/s41467-025-61512-8

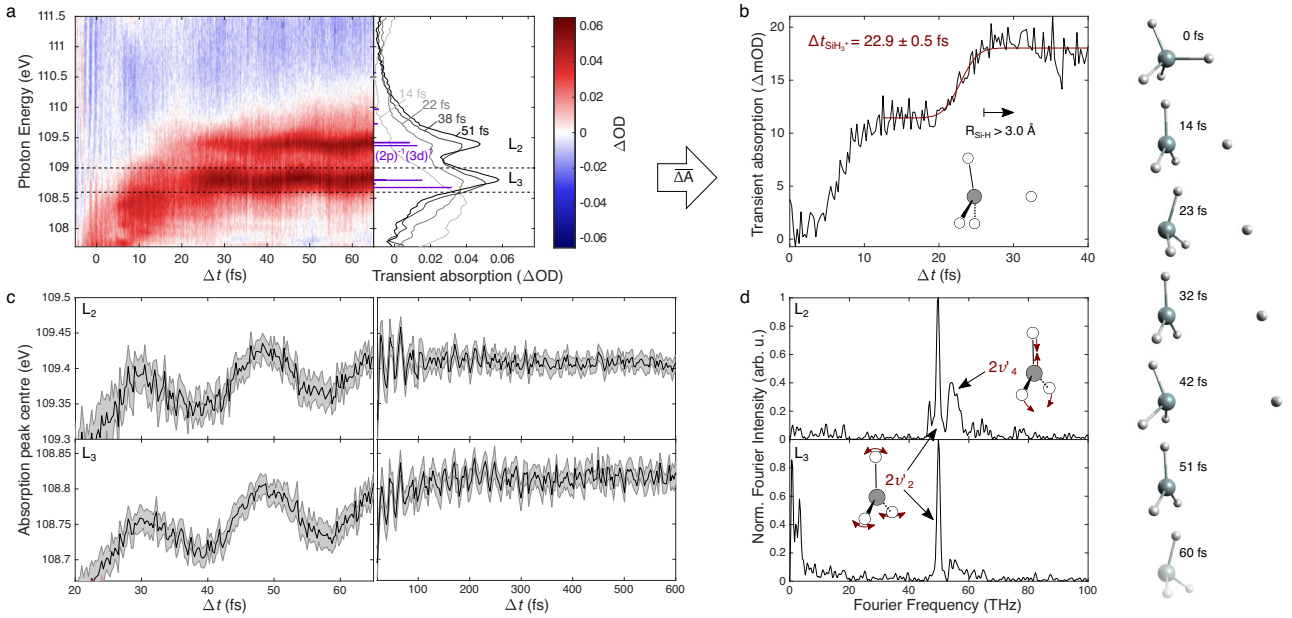

Fig. 2 | The ballistic SiH_3^+ dissociation pathway. a Reanalysed results of a previously-published ATAS measurement[16] showing the ballistic dissociation of SiH_4^+ into SiH_3^+. Snapshots of the absorption spectra are compared with the result of the NEVPT2 calculations (purple bars), assigning the spectral features to 2p → 3d transitions (see Supplementary Section S2.3.1). The integral of the ΔOD between 108.6 and 109.0 eV (dashed horizontal lines) is shown in (**b**), exhibiting two sigmoidal rises. The second rise is assigned to the breaking of the Si–H bond and an error-function fit for $\Delta t > 12.5$ fs yields a SiH_3^+ fragmentation time of $\Delta t_{SiH_3^+} = 22.9 \pm 0.5$ fs. **c** Results of Gaussian fits (95% confidence intervals shown in grey) of transient spectra as a function of Δt (from **a** and Fig. 1b), revealing the post-fragmentation vibrational dynamics of SiH_3^+. Agreement between experiment and AIMD calculations is demonstrated through snapshots (far-right) and in Supplementary Figs. S5 and S6. A Fourier transform, shown in (**d**), reveals the frequency of these beats to be 50 THz, the second harmonic of the 838 cm^{-1} umbrella mode[25].

region centred at 106 eV, a 2p → 3d region centred around 110 eV, and a 2p → Rydberg region centred at 115 eV). ATAS measurements usually focus on the core-valence spectral region as it typically exhibits stronger and broader signals which are easier to calculate. The higher resolution, SNR and self-sufficiency of our methodology, however, allows us to take full advantage of the two higher-energy regions which are usually well-separated from the other absorption features due to the ionisation-induced blue-shift (see Supplementary Section S2.2).

We start with the analysis of the SiH_3^+ channel in Fig. 1b. From symmetry considerations, the breaking of a single Si–H bond must occur through the JT-activation of one or both of the t_2-symmetry vibrational modes. These are the ν_3 anti-symmetric stretch (15 fs period in silane) and the ν_4 umbrella-bending modes (36 fs period in silane). Our experiments manifest both of these modes: the faster ν_3 vibrations are very short lived; they only appear in the experimental results for the first 25 fs after Δt = 0 fs in the central energy of 2p → Rydberg transition at 112 eV. Supplementary Fig. S7 shows how they modulate the energy of these peaks with a period of 7–8 fs.

The results in the second spectral region, magnified in Fig. 2a, exhibit richer dynamics. Over the first 30 fs, its absorption features experience a blue shift as well as modulations in their linewidths. Upon dissociation, the measured transient spectrum narrows and converges to a spin-orbit-split pair of peaks at 108.8 and 109.4 eV characteristic of SiH_3^+ (a comparison between the synchrotron[17] and ATAS results can be found in Fig. 3a). As the 108.8 eV peak does not overlap with the spectra of SiH_2^+, the integrated absorption between 108.6 and 109.0 eV can be used as a transient measure of convergence to SiH_3^+.

The integrated absorption shown in Fig. 2b exhibits two sigmoidal rises; whereas the first is dependent on the exact energy range of the integration because it is a consequence of the blue shift, the second is a result of the changes in linewidth (the origin of which is explored in Supplementary Section S3.4). From an error function fit of this second sigmoid (shown in maroon), the dissociation time of the SiH_3^+ channel is found to be $\Delta t_{SiH_3^+} = 22.9 \pm 0.5$ fs. This result is in agreement with the only published theoretical study on SiH_4^+ fragmentation[24], which has estimated the bond dissociation time (here defined as the time taken to double the bond length) to be roughly 20 fs. To supplement these results we performed our own AIMD simulations (see Supplementary Section S2.4 for more details) which yield a dissociation time of 19 fs.

The experimentally observed dynamics of this first channel do not end with the breaking of the Si–H bond. The SiH_3^+ fragment is expected to retain 750 meV of vibrational energy[24], resulting in long-lived, large-amplitude vibrations. Experimentally, this manifests as clear vibrational quantum beats in the transient-absorption spectra for $\Delta t > 25$ fs. A Gaussian fit of each transient spectrum of both the short and long scan (results shown in Fig. 2d and methodology in Supplementary Section S3.2) reveals that the central energies of the absorption peaks oscillate with a period of 20 fs (50 THz)—twice the frequency of the 838 cm^{-1} (39.8 fs) a''_2-symmetry ν'_2 out-of-plane umbrella mode of SiH_3^+[25].

The excitation of the ν'_2 mode is also seen in AIMD simulations: the AIMD snapshots on the right of Fig. 2 show how the plane containing the three bound hydrogen atoms continues to oscillate above and below the silicon atom despite the hydrogen atom having dissociated after ~25 fs. While we demonstrate numeric agreement between experiment and simulations in Supplementary Figs. S5 and S6, it is important to stress that the conclusions drawn in this work are not dependant on it; which allows the uncoupling of the experimental and theoretical results. The excitation of the ν'_2 mode is also supported when we consider the mapping of the irreducible representation of the SiH_4 ν_4 mode to that of the trigonal-planar SiH_3^+ species: T_2 (T_d) → A_1 (C_{3v}) → A''_2 (D_{3h}). We experimentally observe the second harmonic of the a''_2-symmetry ν'_2 mode due to its symmetry—an equal displacement along the positive or negative direction produces a spectroscopically indistinguishable geometry. The observables of the system therefore only depend on the absolute displacement of the mode, which explains why the observed modulation has half the period of the vibrational mode.

https://doi.org/10.1038/s41467-025-61512-8

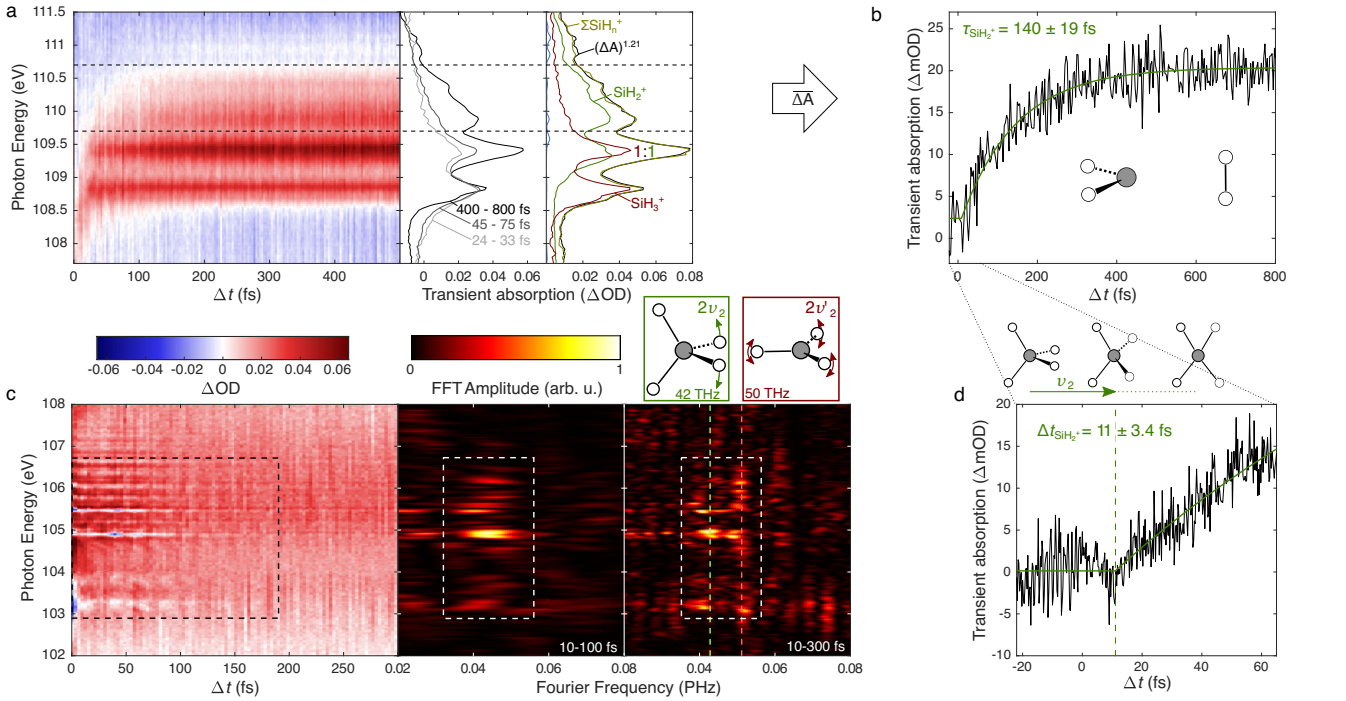

Fig. 3 | The transient SiH_4^+ species and its decay into SiH_2^+. a Results of the longer ATAS measurement (Fig. 1b) showing the SiH_2^+ fragment's transient absorption. The right-hand panel compares time-averaged transient spectra and their non-linear correction $(\Delta A)^{1.21}$ (greyscale) with synchrotron results[17] (coloured). The absorption between 109.7 and 110.7 eV is integrated and plotted as a function of pump-probe delay in (**b**), in which a negative exponential decay fit reveals a 140 ± 19 fs decay constant. **c** The spectral signature and vibrational dynamics of the JT-distorted SiH_4^+ species (highlighted with dashed rectangles). The transient spectrum is produced by applying a 4-THz-wide Fourier filter to the ATAS results, followed by a 33% depletion correction (see Supplementary Section S3.5). The right-hand panels show the result of a Fourier transform over the first 100 fs and 300 fs, respectively, and highlight the strongest Fourier frequencies with dashed vertical lines. The 42 THz signals are caused by ν_2 torsional vibrations (see central inset) and are the experimental signature of the SiH_4^+ species. **d** Shows the integrated absorption from the fine delay scan. A thresholded negative exponential fit reveals the induction time to be 11 ± 3.4 fs.

The amplitude of the oscillations appear to decrease at $\Delta t \sim 100$ fs —two vibrational periods of the ν'_2 umbrella mode. Especially in the case of the 109.4-eV line (upper panel of Fig. 2d), this is followed by a partial rephasing which peaks around a delay of 200 fs, with a lasting dephasing observed after ~400 fs. This sub-picosecond dephasing of the vibrational quantum beat is a result of the anharmonicity experienced by the umbrella-mode wavepacket due to its large-amplitude motion. Further anharmonic effects may be introduced through the Coriolis interaction between the ν'_2 (a''_2) mode and the ν'_4 (e′) H–Si–H rocking/scissoring mode (938 cm^{-1})[25,26]. This is supported by the appearance of the ν'_4 mode's second harmonic (56 THz) in the Fourier spectra, particularly in that of the higher-energy L_2 absorption line (we attributed this selectivity to the fact that, unlike the L_3, the L_2 transition dipole vector has components in the plane of the molecule).

We now move to the second channel: $SiH_4^+ \rightarrow SiH_2^+ + H_2$. As with SiH_3^+, the $L_{2,3}$ absorption spectrum of the SiH_2^+ can be obtained from synchrotron studies[17]. By taking advantage of these absolute cross sections, it is even possible to determine the relative abundance of the two fragments directly from the transient spectra at long delays. Through minimizing the difference between the measured spectrum and a weighted sum of synchrotron spectra (right panel of Fig. 3a), we find the ratio of abundance to be 1:1, in agreement with our TOF-MS results and the single-photon-ionisation literature. This analysis relies on a correction to account for the fact that the pump's focus is smaller than the probe's (discussed further in Supplementary Section S3.6).

Next, we compare the structure of the two cationic species' XAS. Owing to its lower C_{2v} symmetry, SiH_2^+ exhibits more distinct core-valence transitions than SiH_3^+, leading to a broad congested XAS between 109 and 111 eV. The SiH_2^+ species' featureless absorption tail between 109.7 and 110.7 eV exhibits minimal overlap with the XAS of SiH_3^+, allowing us to use this spectral region as a probe of the abundance of the SiH_2^+ species. In contrast to the sigmoid-like temporal evolution of the SiH_3^+ absorption, that of SiH_2^+ (shown in Fig. 3b) is found to be well described with a negative exponential decay, signifying that the dissociation of SiH_4^+ to SiH_2^+ is limited by a first-order stochastic process[27]. From a least-squares fit we obtain a decay constant for the SiH_2^+ dissociation (and therefore the lifetime of a metastable SiH_4^+ species) measuring $\tau_{SiH_2^+} = 140 \pm 19$ fs.

Whereas the picosecond-spanning measurement probes the stochastic lifetime of the unstable SiH_4^+ fragment, the finer delay-step measurement reveals a finite induction time $\Delta t_{SiH_2^+}$ for the reaction. Corresponding experimentally to the delay at which the integrated absorption shows the first sign of change, it reveals the time taken for the system to rearrange into the metastable SiH_4^+ and therefore sheds light on the reaction path. From a least-squares fit of the integrated absorption using a thresholded negative exponential decay (see Supplementary Section S3.3 for details), we find that this amounts to $\Delta t_{SiH_2^+} = 11 \pm 3.4$ fs.

Note that the stark difference in timescales and absence of the stochastic temporal evolution in the 108.6–109.0 eV spectral region is proof that the metastable SiH_4^+ species that leads to the SiH_2^+ fragment does not decay into SiH_3^+. Given the speed of the competing SiH_3^+ reaction and the existence of the induction time, the bifurcation must occur very early in the reaction, in close vicinity to the Frank-Condon point, and the paths of the two wavepackets must not re-cross (indicated by a red cross in Fig. 4).

Additional insight into the SiH_2^+ dissociation mechanism can be gained by identifying the transient signals of the metastable SiH_4^+ species. Perhaps due to the species' low symmetry or large-amplitude motion, no clear SiH_4^+ 2p → 3d/Rydberg absorption features are

https://doi.org/10.1038/s41467-025-61512-8

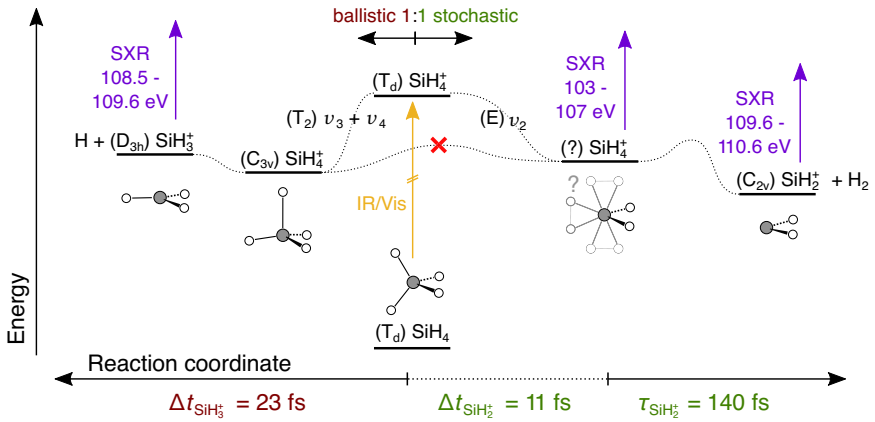

Fig. 4 | Schematic of the bifurcating reaction. The relevant local minima of the SiH_4^+ system (from ref. 36) are plotted as a function of energy vertically and according to the reaction path horizontally. The symmetry and geometry of each minima is also shown. The dotted curves represent the reaction paths that transform one geometry into another and are labelled according to the symmetry of the vibrational mode (in the T_d point group) that dominates them. The strong-field ionisation of the pump pulse is represented by the orange arrow while the purple arrows represent the probing of the different states with the delayed isolated attosecond SXR pulse. The spectral regions in which the respective state absorb are indicated as well. The experimentally determined timescales of the reactions are specified at the bottom of the figure.

observed in the experimental results. As we will show next, however, the stronger 2p → antibonding transitions do appear. The synchrotron measurements reveal where these stronger SiH_4^+ transients can be expected: Supplementary Fig. S12 compares the $L_{2,3}$-edge of SiH_n^+ for $n = 1–3$ indicating that, for $n = 4$, one would expect absorption between 103 and 108 eV. This spectral region exhibits a large overlap with the absorption of the neutral silane species, where strong depletion and ground state vibrational dynamics are already present. To uncover the SiH_4^+ signals these must be removed. The ground-state bleach is corrected by applying a constant 33% depletion correction, while the 15-fs vibrational dynamics of the ground state are removed using a Fourier filter (see Supplementary Section S3.5 for more details). The resulting ground-state-free transient spectra are shown in Fig. 3c, which reveal previously obscured vibrational transients between 103 and 107 eV that decay over the first 100–150 fs.

An FFT over the first 100 fs (middle panel of Fig. 3c) reveals the dominant frequency of these short-lived signals to be between 40 and 50 THz. A longer, higher-resolution FFT (right-hand panel) shows that these signals can be separated in both Fourier frequency and spectral energy. One weaker signal is mostly located below photon energies of 105 eV and exhibits a 50 THz Fourier frequency, matching the ν'_2 quantum beats of the SiH_3^+ fragment and therefore corresponding to the core-antibonding transients of the SiH_3^+ species. A second signal exhibits a new Fourier frequency at 42 THz, which is found to be particularly strong at a photon energy of 104.9 eV and more weakly at 103.2 and 105.4 eV. We assign this to the metastable SiH_4^+ species. Note that these vibrational signals appear in close spectral proximity to the much higher frequency electronic quantum beats discussed in our previous work[16] (whose dominant electronic beats appear at 105.6 and 106.1 eV). The signals, however, are unrelated: the sub-100 meV resolution of our instrument clearly spectrally distinguishes them.

The 42 THz frequency of this quantum beat, together with the induction time of 11 fs identifies the reaction path of the second channel (see Fig. 4). Given the symmetry of the system and the vibrational mode, we expect the observed beats to exhibit the second harmonic of the vibrations they originate from (as is also the case for SiH_3^+). 21 THz falls into the typical range for H–Si–H torsion modes[28] and matches the weak 93 meV (22.5 THz) vibronic progression in the photoelectron spectrum of silane[29], which has been assigned to the E-symmetry ν_2 torsion/scissoring mode with MCTDH simulations[30] (see inset above Fig. 3c). Meanwhile, the 11-fs induction time being a quarter of this vibrational period reveals that the dissociation begins once the vibrational wavepacket has reached the local minimum of the PES along the ν_2 mode. At this point, a stochastic decay process must become activated which gradually depletes the population of the SiH_4^+ species yielding the dissociated SiH_2^+ product.

It is important to emphasise the unique insight offered by these results. Not only are the timescales and vibrational modes involved in the $SiH_4^+ \rightarrow SiH_2^+ + H_2$ chemical transition revealed, but the moment when the compact vibrational wavepacket decoheres is also resolved. From this point on, the reaction proceeds stochastically with no ability to preserve coherence.

Attempts at reproducing the SiH_2^+ channel's observed dynamics with AIMD have revealed the limitations of classical-trajectory calculations. Of the 50 trajectories calculated in their study, Tachikawa[24] found only one that yielded SiH_2^+. Our own AIMD results, employing 1000 trajectories with initial conditions sampled from a thermal Wigner distribution (rather than the purely thermal distribution used by Tachikawa), yielded an even lower probability of SiH_2^+ formation (only 1.4% at 300 K). When the trajectories were sampled at 3000 K, this fraction only increased to 12.9%. These results are clearly inconsistent with the approximately equal branching observed experimentally. Since adiabatic semi-classical AIMD trajectories do not reproduce the dynamics of the SiH_2^+ dissociation channel, excited-state dynamics, non-adiabatic dynamics and nuclear quantum effects (such as tunnelling or above-barrier reflection) may be possible explanations for this discrepancy.

This study has shown how the unmatched temporal and energy resolution of our novel approach coupled with the self-sufficiency provided by the in-situ MS yields unprecedented insights into the fastest structural dynamics occurring in nature. Taking the Jahn–Teller driven dissociation of SiH_4^+ as an example, we completely resolved and disentangled the quantum dynamics of a bifurcating wave packet, shedding new light on the mechanisms involved. As a result, this study has provided the first spectroscopic observation of the transient SiH_4^+ molecule, including its vibrational dynamics and bifurcating reaction paths. It has revealed that the dissociation into $SiH_3^+ + H$ proceeds ballistically in 22.9 ± 0.5 fs and coherently excites the umbrella motion of SiH_3^+. It has also revealed that the dissociation into $SiH_2^+ + H_2$ proceeds stochastically with a time constant of 140 ± 19 fs, but only after a finite induction time of 11 ± 3.4 fs. The failure of AIMD at reproducing both the $[SiH_2^+]$:$[SiH_3^+]$ branching ratio and the detailed dynamics of the $SiH_2^+ + H_2$ channel offers both a notable challenge and a unique benchmark for future quantum-dynamical simulations.

These findings on the JT effect in SiH_4^+ are not only fundamentally important, they also answer questions of industrial relevance; the fragmentation dynamics of SiH_4^+ are relevant to our understanding of silane plasmas and how they form high-purity amorphous silicon films[31], a critical process in the production of low-cost photovoltaic cells and thin-film transistors[32].

Looking forward, this study demonstrates the importance of single-femtosecond temporal resolution for the complete characterisation of vibrational dynamics, further developing our understanding of the competing mechanisms that underlie them. The unprecedented capabilities of such experiments can now be extended to more complex systems, such as metal complexes to better understand the mechanisms that govern photocatalysis[33], and to light-induced superconductors[34,35] for elucidating the quantum-mechanical primary processes controlling such phenomena.

Methods

Attosecond transient absorption spectroscopy

The ATAS experiment is driven with a 5.2 fs FWHM optical pulse spanning 500–1000 nm, generated by spectrally broadening the compressed output of a FEMTOPOWER V CEP titanium:sapphire laser system. This few-cycle pulse serves as both the pump pulse as well as the driving pulse for high harmonic generation (HHG). HHG is performed in helium to generate the attosecond soft-X-ray probe pulses exhibiting a continuous spectrum at the silicon $L_{2,3}$-edge. The attosecond delay between the pump and probe pulses is controlled using a custom-built attosecond interferometer. The pump and probe pulses pass through the target gas (Silane 5.0 from Linde) in a 1 cm-long target cell. The transmitted X-ray spectra are measured using a Hitachi 001-0660 flat field grating and a Princeton Instruments PIXIS-XO 2KB X-ray camera. For more details see Supplementary Section S1.1.

Time-of-flight mass spectrometry

The same few-cycle pump pulse used for ATAS is also used to perform in-situ mass spectrometry. The target chamber is filled with silane through the ATAS target and a large potential is applied to it, accelerating the cations created through strong-field ionisation towards a Photonis MigaSpiraltron channeltron where their arrival time is recorded. For more details see Supplementary Section S1.2.

Ab-initio molecular dynamics

AIMD simulations of SiH_4^+ were performed using Q-Chem 4.3 at the CISD/6-311G(d,p) level of theory using a 0.1 fs timestep. The initial conditions (geometries and momenta) for the AIMD simulations were generated from a Wigner distribution of the SiH_4 ground state using the `wigner.py` function from SHARC3.0. For more details see Supplementary Section S2.3.

Calculation of X-ray absorption spectra

The ab-initio XAS spectrum of SiH_3^+ was obtained at the SC-NEVPT2/def2-QZVPP level of theory. The geometry used for the calculation was trigonal planar (D_{3h}) with an Si–H bond length of 1.46 Å. This was taken from an experimental vibrational study of SiH_3^+ [25]. For more details see Supplementary Section S2.2.1.

Reporting summary

Further information on research design is available in the Nature Portfolio Reporting Summary linked to this article.

Data availability

Source data is available at ETH Zurich's Research Collection under the https://doi.org/10.3929/ethz-b-000737533.

References

1. Bersuker, I. B. *The Jahn-Teller effect*. (Cambridge University Press, Cambridge, UK, 2006).
2. Wörner, H. J. & Merkt, F. Jahn-teller effects in molecular cations studied by photoelectron spectroscopy and group theory. *Angew. Chem. Int. Ed.* **48**, 6404–6424 (2009).
3. Jahn, H. A. & Teller, E. Stability of polyatomic molecules in degenerate electronic states-i-orbital degeneracy. *Proc. R. Soc. Lond. Ser. A Math. Phys. Sci.* **161**, 220–235 (1937).
4. Zadik, R. H. et al. Optimized unconventional superconductivity in a molecular jahn-teller metal. *Sci. Adv.* **1**, e1500059 (2015).
5. Paddon-Row, M., Fox, D., Pople, J., Houk, K. & Pratt, D. W. Dynamic Jahn-Teller effect in methane radical cation. location of the transition structures for hydrogen scrambling and inversion. *J. Am. Chem. Soc.* **107**, 7696–7700 (1985).
6. Wörner, H. J., van der Veen, R. & Merkt, F. The Jahn-Teller effect in the methane cation: rovibronic structure and the geometric phase. *Phys. Rev. Lett.* **97**, 173003 (2006).
7. Ridente, E. et al. Femtosecond symmetry breaking and coherent relaxation of methane cations via x-ray spectroscopy. *Science* **380**, 713–717 (2023).
8. Zinchenko, K. S. et al. Few-femtosecond electronic and structural rearrangements of CH_4^+ driven by the Jahn–Teller effect. *Struct. Dyn.* **10**, 064303 (2023).
9. Gonçalves, C. E., Levine, R. & Remacle, F. Ultrafast geometrical reorganization of a methane cation upon sudden ionization: an isotope effect on electronic non-equilibrium quantum dynamics. *Phys. Chem. Chem. Phys.* **23**, 12051–12059 (2021).
10. Pertot, Y. et al. Time-resolved x-ray absorption spectroscopy with a water window high-harmonic source. *Science* **355**, 264–267 (2017).
11. Ross, A. D. et al. Jahn-Teller distortion and dissociation of CCl_4^+ by transient X-ray spectroscopy simultaneously at the carbon K- and chlorine L-edge. *Chem. Sci.* **13**, 9310–9320 (2022).
12. Valtazanos, P. & Ruedenberg, K. Bifurcations and transition states. *Theoretica Chim. acta* **69**, 281–307 (1986).
13. Ando, T. et al. Wave packet bifurcation in ultrafast hydrogen migration in CH_3OH^+ by pump-probe coincidence momentum imaging with few-cycle laser pulses. *Chem. Phys. Lett.* **624**, 78–82 (2015).
14. Wei, Z. et al. Elucidating the origins of multimode vibrational coherences of polyatomic molecules induced by intense laser fields. *Nat. Commun.* **8**, 735 (2017).
15. Kobayashi, Y., Chang, K. F., Zeng, T., Neumark, D. M. & Leone, S. R. Direct mapping of curve-crossing dynamics in IBr by attosecond transient absorption spectroscopy. *Science* **365**, 79–83 (2019).
16. Matselyukh, D. T., Despré, V., Golubev, N. V., Kuleff, A. I. & Wörner, H. J. Decoherence and revival in attosecond charge migration driven by non-adiabatic dynamics. *Nat. Phys.* **18**, 1206–1213 (2022).
17. Kennedy, E. et al. Evolution of l-shell photoabsorption of the molecular-ion series SiH_n^+(n= 1, 2, 3): Experimental and theoretical studies. *Phys. Rev. A* **97**, 043410 (2018).
18. Goll, E., Wunner, G. & Saenz, A. Formation of ground-state vibrational wave packets in intense ultrashort laser pulses. *Phys. Rev. Lett.* **97**, 103003 (2006).
19. Timmers, H. et al. Disentangling conical intersection and coherent molecular dynamics in methyl bromide with attosecond transient absorption spectroscopy. *Nat. Commun.* **10**, 1–8 (2019).
20. Hogness, T. R. & Kvalnes, H. M. The ionization processes in methane interpreted by the mass spectrograph. *Phys. Rev.* **32**, 942 (1928).
21. Cooper, G., Ibuki, T. & Brion, C. Absolute oscillator strengths for photoabsorption, photoionization and ionic photofragmentation of silane. I. The valence shell. *Chem. Phys.* **140**, 133–145 (1990).
22. Basner, R., Schmidt, M., Tarnovsky, V., Becker, K. & Deutsch, H. Dissociative ionization of silane by electron impact. *Int. J. Mass Spectrom. Ion-. Process.* **171**, 83–93 (1997).

23. Püttner, R., Domke, M., Lentz, D. & Kaindl, G. Si 2p photoabsorption in SiH_4 and SiD_4 : Molecular distortion in core-excited silane. *Phys. Rev. A* **56**, 1228–1239 (1997).
24. Tachikawa, H. A full dimensional ab initio direct trajectory study on the ionization dynamics of SiH4. *Phys. Chem. Chem. Phys.* **4**, 1135–1140 (2002).
25. Davies, P. B. & Smith, D. M. Diode laser spectroscopy and coupled analysis of the v_2 and v_4 fundamental bands of SiH_3^+. *J. Chem. Phys.* **100**, 6166–6174 (1994).
26. Green, W. H., Jayatilaka, D., Willetts, A., Amos, R. D. & Handy, N. C. The prediction of spectroscopic properties from quartic correlated force fields: HCCF, HFCO, SiH_3^+. *J. Chem. Phys.* **93**, 4965–4981 (1990).
27. Krieger, I. M. & Gans, P. J. First-order stochastic processes. *J. Chem. Phys.* **32**, 247–250 (1960).
28. Hawkins, J. A. & Wilson, M. K. The infrared and raman spectra of SiH_2Cl_2. *J. Chem. Phys.* **21**, 360–362 (1953).
29. Potts, A. W. & Price, W. C. The photoelectron spectra of methane, silane, germane and stannane. *Proc. R. Soc. Lond. A. Math. Phys. Sci.* **326**, 165–179 (1972).
30. Mondal, T. & Varandas, A. J. Silane radical cation: a theoretical account on the Jahn-Teller effect at a triple degeneracy. *J. Phys. Chem. A* **117**, 8794–8805 (2013).
31. Nguyen, T. N., Lee, Y. M., Wu, J. S. & Lin, M. C. Ab initio chemical kinetics for the thermal decomposition of SiH_4^+ ion and related reverse ion-molecule reactions of interest to PECVD of a-Si:H films. *Plasma Chem. Plasma Process.* **37**, 1249–1264 (2017).
32. Street, R. *Hydrogenated amorphous silicon*. Cambridge Solid State Science Series (Cambridge University Press, 1991).
33. Chergui, M. Ultrafast photophysics of transition metal complexes. *Acc. Chem. Res.* **48**, 801–808 (2015).
34. Fausti, D. et al. Light-induced superconductivity in a stripe-ordered cuprate. *science* **331**, 189–191 (2011).
35. Mitrano, M. et al. Possible light-induced superconductivity in K_3C_{60} at high temperature. *Nature* **530**, 461–464 (2016).
36. Paddon-Row, M. N. & Wong, S. S. On the structure of the SiH_4^+ cation and its potential energy surface for rearrangement and dissociation: an ab initio M.O. study. *J. Chem. Soc. Chem. Commun.* **20**, 1585–1587 (1987).

Acknowledgements

We thank A. Schneider and M. Seiler for their technical support, D. Hammerland for laser maintenance and operation support and S. Danzi for the coating of beamline optics. We gratefully acknowledge funding from an ERC Consolidator Grant (Project No. 772797-ATTOLIQ), and projects 200021_172946, 200020_204298 as well as the NCCR-MUST, funding instruments of the Swiss National Science Foundation. V.S. acknowledges funding from The Czech Science Foundation (Project No. 24-10298M).

Author contributions

H.J.W. conceived the study and supervised the work. D.T.M. performed the experiment and analysis. V.S. performed the AIMD calculations. D.T.M. performed the NEVPT2 calculations. D.T.M. and H.J.W. wrote the manuscript. All authors contributed to the interpretation of the results and editing of the manuscript.

Competing interests

The authors declare no competing interests.

Additional information

Supplementary information The online version contains supplementary material available at https://doi.org/10.1038/s41467-025-61512-8.

Correspondence and requests for materials should be addressed to Hans Jakob Wörner.

Peer review information *Nature Communications* thanks the anonymous reviewer(s) for their contribution to the peer review of this work. A peer review file is available.